Reaction-Diffusion Algorithm for Quantitative Analysis of Periodic V-Shaped Bundles of Hair Cells in the Inner Ear

Hiroto Shoji*, Ryo Iwamoto

Department of Science and Technology, Kwansei Gakuin University, Sanda, Hyogo, Japan
Email: *shoji@kwansei.ac.jp

Abstract

Columnar outer hair cells of the inner ear form V-shaped bundles, which are arranged in three rows in the cochlea. If the formation of these V-shaped bundles is disturbed, sensorineural hearing loss occurs. To quantify the distribution of V-shaped bundles, the use of a Turing-type reaction-diffusion (RD) system, including anisotropic diffusion, should be considered. We found that a periodic triangle pattern appears based on the anisotropy in the RD system. Then, using the proposed RD system, the image of the V-shaped bundle was examined. The results showed that the correlation between the RD pattern and V-shape bundles not only classifies the experimental result but also significantly differs in the number of directional changes in a set of V-shape bundle. Therefore, this process can help quantify the images of V-shaped bundles.

Keywords

Reaction-Diffusion, Turing, Triangle, Inner Ear

1. Introduction

Although diffusion processes generally generate a uniform distribution of substances, Turing [1] has demonstrated that spatially heterogeneous patterns can be formed out of a completely homogeneous field, in which more than two types of diffusible substances react with one another and engage in random diffusion. When these models are analyzed on a two-dimensional (2D) plane, striped patterns in addition to the spotted patterns emerge [2] [3], which is considered as the basic mechanism. A series of studies on Turing-type reaction-diffusion (RD) systems have been conducted to explain many examples of pattern formation in

chemical reactions [2] [4] and biological processes [3] [5].

Furthermore, many researchers have become interested in developing methods for applying RD systems to image information processing. Admatzky *et al.* [6] have proposed an algorithm for segmenting 2D images, and Ito *et al.* [7] have developed an algorithm for repairing the blurred part of the fingerprints using RD models. In our previous studies, we applied these mechanisms to segment 3D images of the vascular system in the liver [8] [9]. Using these methods with the Turing-type RD system, no preprocessing for noise removal is required, which often affects the accuracy of information extraction.

Outer hair cells inside the cochlea of the inner ear amplify the movement of the basement membrane [10] [11]. The amount of amplification is exquisitely regulated at a frequency close to the characteristic frequency of the location on the basement membrane where the hair cells are located [10] [12] [13]. However, the exquisite formation of hair cells goes astray due to various factors, such as genetic mutations affecting the structures of the inner ear and environmental insults, including noise, ototoxic substances, and hypoxia, resulting in sensorineural hearing loss, which is the most common type of hearing loss worldwide [13] [14] [15].

Outer hair cells are arranged in three rows near the saccule [13] [14]. Columnar outer hair cells form a V-shaped bundle of stereocilia (**Figure 1**), and bundle deformations occur when sensorineural hearing loss occurs (**Figure 1(b)**) [13] [14] [15]. To quantify these deformations, various factors, such as changes in the bundle direction or the number of stereocilia, have been considered. However, given that outer hair cells are arranged in an exquisite balance relative to the surrounding cells and environment [14] [15], measuring the direction of bundles or counting the number of stereocilia is insufficient.

In this study, we developed a new method for quantifying the arrangement of V-shaped bundles of stereocilia using the information obtained from the RD model. Although the RD system generates striped patterns or spotted patterns, we found that periodic triangular patterns are generated in an RD system using anisotropic diffusion. Then, we applied this system to quantify the image of a V-shaped bundle of stereocilia.
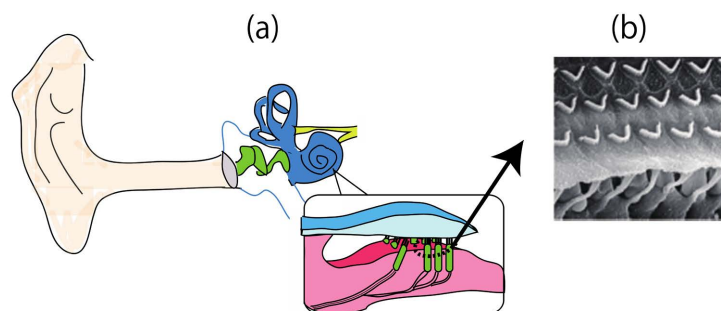

Figure 1. (a) Schematic structure of the inner ear; (b) Schematic representation of the surface of the organ of Corti. The three rows of outer hair cells. Each hair bundle forms a V-shaped bundle [reproduced from [12]].

In this study, first, we explored an RD system, in which triangular patterns are generated. Then, using this RD system, an index for comparing the obtained patterns with the image is prepared. Hence, we propose an algorithm for quantifying the difference between the images. Then, we showed the qualitative differences between the obtained images. Moreover, by preparing the stepwise deformation pattern, obtained via image analysis of a part of the control pattern, we discussed the changes in the index of the images.

2. Methods

2.1. RD Model

Image analysis was performed using an algorithm based on the Turing-type RD model. Turing has shown that two diffusive and reactive materials can generate spatially periodic patterns in a uniform field. The basic model can be expressed as follows:

$$u_t = D_u \nabla^2 u + f(u, v), \tag{1}$$

$$v_t = D_v \nabla^2 v + g(u, v), \tag{2}$$

where u and v denote the densities of the diffusive and reactive materials, respectively, and constants D_u and D_v are all positive. Turing [1] said that if, in the absence of diffusion term (the first terms on the right side in (1) and (2)), u and v of the corresponding ordinary differential equations tend to a linear stable uniform steady state, then under certain conditions spatially inhomogeneous patterns can evolve by diffusion-driven instability if the diffusion coefficients are different ($D_u \neq D_v$). This novel concept is now called "diffusion-driven instability" or "Turing instability" [2] [3].

To satisfy the conditions of Turing instability, the following four conditions are required. Equations (1) and (2) have a time-independent uniform solution (u_0, v_0), which satisfies $f(u_0, v_0) = 0$ and $g(u_0, v_0) = 0$. Since the steady state is stable (u_0, v_0) in the reaction terms in Equation (1), we have $f_u + g_v < 0$ and $f_u g_v - f_v g_u > 0$. The partial derivatives are evaluated. Then, the steady-state (u_0, v_0) becomes unstable when $D_v f_u + D_u g_v > 0$ and $(D_v f_u g_v - D_u f_v g_u)^2 - 4D_u D_v (f_u g_v - f_v g_u) > 0$ is satisfied. The model satisfying these conditions generates spatially periodic patterns from a uniform distribution.

The equation of FitzHugh-Nagumo [16] selected the following reaction terms:

$$f(u, v) = u - u^3 - v, \tag{3}$$

$$g(u, v) = \gamma(u - \alpha v - \beta), \tag{4}$$

where the parameters α, β and γ are all positive, and are selected to satisfy the four conditions. Following this mechanism, in an area where activator u is a little more than around, the high activation of u is antagonized by a high inhibition of v. The high activator u becomes even higher since the inhibition spread faster than u. On the other hand, by the faster diffusion, inhibitor v preempts an area

where u is less, and inhibits u's activation. In this way, small differences become more pronounced, then the periodic pattern are self-organized.

When these models are analyzed on a 2D plane, as opposed to on a 1D line, striped patterns in addition to spotted patterns often emerge [2] [17], which is considered as the basic mechanism, explaining many examples of striped patterns observed in animal coatings [3].

2.2. RD Model with Anisotropy

The evaluation of patterns is based on an RD model with anisotropy. Here we introduce the anisotropic diffusion following the method introduced by Kobayashi [18] and Shoji *et al.* [19]. According to the planar cell polarity of hair cell [10] [11] [12], we assumed that the diffusion coefficient of u depends on the direction of flux u as follows:

$$u_t = d_u \nabla \cdot \left(D_u \left(\theta_u \right) \nabla u \right) + u \left(1 - u^2 \right) - v,$$ (5)

$$v_t = d_v \nabla^2 v + \gamma \left(u - \alpha v - \beta \right).$$ (6)

The diffusion coefficient of u is as follows:

$$D_u \left(\theta_u \right) = \frac{1}{\sqrt{1 - \delta_u \cos 3\theta_u}}$$ (7)

where θ_u denotes the angle of the gradient vectors of u, which can be expressed as follows:

$$\theta_u = \arctan \left(\frac{\partial u}{\partial y} \middle/ \frac{\partial u}{\partial x} \right).$$

The flux of u is proportional to the gradient vector; however, the multiplication coefficient depends on the angle of the vector. Equation (7) implies that the diffusivity of u is the highest for $\theta_u = 0, \frac{2\pi}{3}$, and $\frac{4\pi}{3}$. δ_u denotes the magnitude of the anisotropy of u. This satisfies $0 \le \delta_u \le 1$. A case $\delta_u = 0$ implies the isotropic diffusion.

Figure 2 shows the time evolution of the distribution of u in two dimensions. The model given by Equations (5)-(7) was numerically calculated. The following parameters were selected: $\alpha = 0.50, \beta = 0.01, \gamma = 26.0, d_u = 0.0001$ and $d_v = 0.01$. All the simulations were performed using periodic boundary conditions in a rectangular domain of size: 2.42×1.42 (grid size: 242×142). A simple explicit scheme was adopted. The mesh size of time was set as 10^{-6} to adopt the stability condition for the numerical analysis. In the case where $\delta_u = 0.00$, no anisotropic diffusion affected the patterns; that is, native Turing patterns emerged. Figures 2(a)-(c) shows the time evolution of the distribution of u. The distribution of v is the same periodic pattern that has the same period but different the amplitude. The model generated a striped pattern in which white areas indicate a high u value and the black areas were in lines parallel to each other.

To quantify the V-shaped bundle, we consider a system that includes anisotropic diffusion ($\delta_u > 0$) in which periodic triangular patterns form. In the case
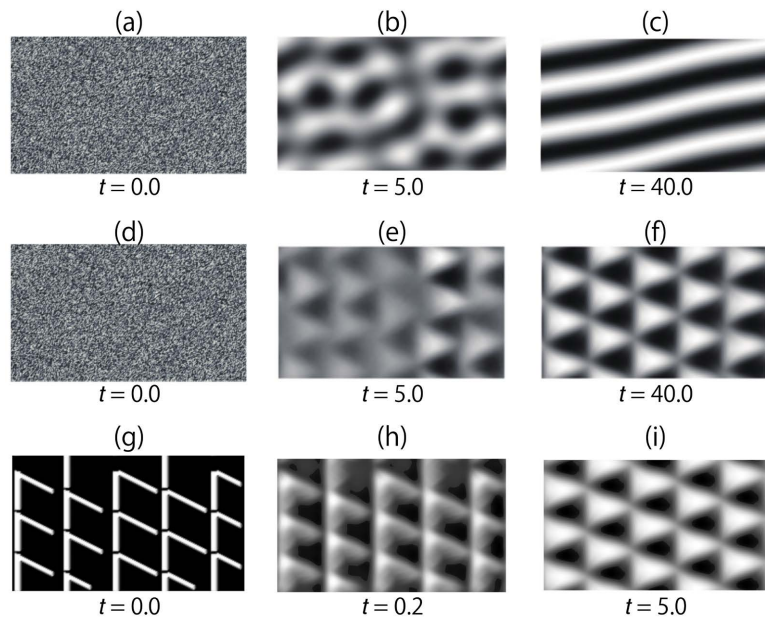
Figure 2. Time evolution of $u(\vec{x}, t)$. (a)-(c) were numerically obtained from Equation (1) using $\delta_u = 0.00$; (d)-(f) were obtained using $\delta_u = 0.90$; and (g)-(i) were self-organized under given initial distribution shown in (g) for the same with $\delta_u = 0.90$. Given that the patterns in (g)-(i) were generated much faster than those in (a)-(c) or (d)-(f), the times of the patterns are different between (b) (or (e)) and (h), and between (c) (or (f)) and (i).

where $\delta_u = 0.90$, **Figures 2(d)-(f)** show the time evolution of the distribution of *u*. The triangular modes initially appeared spontaneously (**Figure 2(e)**), and then, the triangular mode adjusted the location to each other and arranged regularly (**Figure 2(f)**). As in the preceding section, we set the parameter as $\delta_u = 0.90$.

The Turing-type RD model can perform image processing tasks, such as enhancement and restoration [7]. By considering the case in which local differences in the intensities of the images of V-shaped bundles exist, we set the initial distribution of *u* in which white areas indicate of a high *u* value (equal to 0.5), and the black areas indicate a low *u* value (**Figure 2(g)**). We applied the proposed RD model to the prepared initial distribution. **Figures 2(g)-(i)** show the time evolution of the obtained distribution of *u* based on the proposed RD model. The triangles were formed in the direction aligned to the two edges of the V-shaped bundle. Using this property, we performed image analysis to quantify the distribution of the outer cells.

2.3. Algorithm for Selection

Figure 3 shows a diagram of the image analysis used to quantify the distribution of the outer cells. First, we linearly scaled the [0, 255] gray-scale image of the V-shaped bundle on a range of −0.5 to 0.5. Let $U(\vec{x})$ be a scaled distribution. The initial conditions of *u* and *v* were multiplied with the distribution of $U(\vec{x})$ and 0.1 with a small random deviation. Subsequently, an RD system with anisotropic
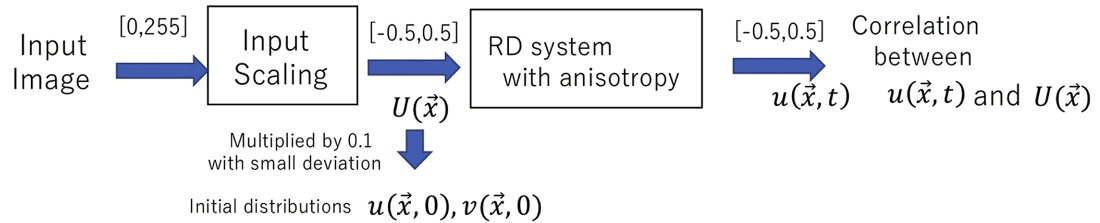
Figure 3. RD algorithm diagram.

diffusion was numerically performed. After the computation, we calculated the correlation between u and U was calculated as follows:

$$I = 1/\left(S\sigma_u\sigma_U\right)\int\left(u(\vec{x})-\bar{u}\right)\left(U(\vec{x})-\bar{U}\right)\mathrm{d}\vec{x} \qquad (8)$$

where $\bar{u}, \bar{U}, \sigma_u$ and σ_U denote the mean and variance of u and U. S is the total area. For each image, the correlation was calculated using Equation (8).

2.4. Statistical Analysis

The results were evaluated using the Kruskal-Wallis test followed by the Mann-Whitney U-test. These statistical analyses were performed using R in a Macintosh system.

3. Results

3.1. Comparison between Control and Disturbed Images and Numerically Obtained Patterns

Figure 4(c) shows the results for the patterns obtained from the initial distributions provided in **Figure 4(a)**. **Figure 4(c)** shows the output image at time 10.0. Although the orientation of the V-shaped bundle in **Figure 4(a)** is the same, every V-shaped bundle seemed to maintain a delicate balance and its own combination among bundles. The RD system with the anisotropy of Equations (5)-(7) captured these properties of the V-shaped bundle, where the directions of the triangles appeared were the same; however, the triangles were subtly arranged in a balanced manner between each other. The correlation (Equation (8)) between the scaled distribution $U(\vec{x})$ of **Figure 4(a)** and the numerically obtained distribution of **Figure 4(c)** corresponded to 5.68×10^{-2}.

Figure 4(d) shows the patterns obtained from the initial distributions provided in **Figure 4(b)**. The orientation of the triangles in the obtained images was $\pi/3$ diagonally to the right. Although the orientation of a few bundles was the same as that of a triangle in the obtained numerical pattern, most orientations of other V-shaped bundles were misaligned. Therefore, the correlation between $U(\vec{x})$ in **Figure 4(b)** and the numerically obtained distribution in **Figure 4(g)** was 2.93×10^{-2}, which was lower than the control.

The five samples listed in **Table 1** were tested, and the results of the correlation are shown in **Table 1**. Using the proposed index (the correlation of Equation (8)), the difference can be clearly observed.
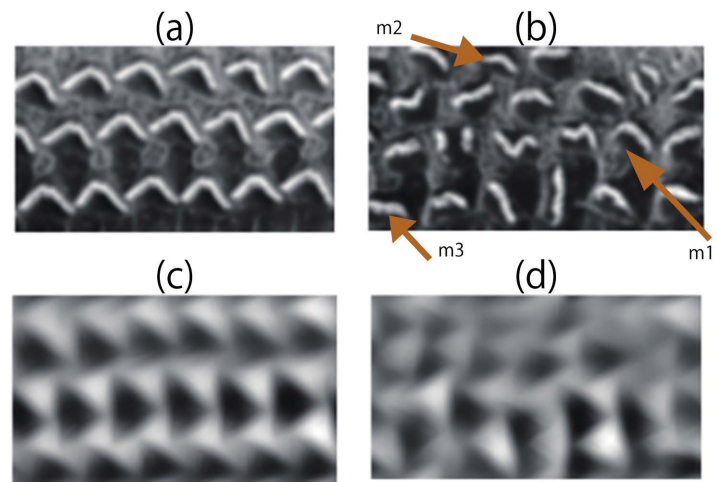
Figure 4. (a) (b) Examples of images examined reproduced from the Ref. [14]. (c) (d) Patterns obtained from (a) and (b) via the RD processing of Equation (2) using $\delta_u = 0.90$ using the initial distributions in (a) and (b), respectively. The brown arrows in (b) indicate the transformation points performed in Section 3.3.

Table 1. Comparison of the correlation I of Equation (8). * indicates the figure shown in **Figure 4(a)**, and ** indicates the figure shown in **Figure 4(b)**.

Paper	Control Figure No.	Correlation I	Corresponding Figure No.	Correlation I
Forge A. *et al.* [14]	**Figure 1(b)***	5.68×10^{-2}	**Figure 1(c)***	2.93×10^{-2}
Siletti K. *et al.* [23]	**Figure 1(d)** left	5.31×10^{-2}	**Figure 1(d)** right	3.59×10^{-2}
	Figure 3(a) upper		**Figure 3(a)** lower	
Ozono Y. *et al.* [24]	Left	5.54×10^{-2}	Left	3.24×10^{-2}
	Middle	5.06×10^{-2}	Middle	3.21×10^{-2}
	Right	5.11×10^{-2}	Right	3.91×10^{-2}

3.2. Gradual Changes in the Orientation of the V-Shaped Bundles in Images and Their Score Changes

Image analysis was performed to measure the quantitative differences during modified changes in the differences. Using the images used in **Figure 2**, the image transformation was performed as follows. In the control image (**Figure 2(a)**), the bundle was randomly selected, and the selected area was rotated π/2 or 3π/2. Then, the rotated area was embedded in the same image. **Figure 5(a)** shows an example of a single-area transformation. The white circle indicates the transformed area. **Figure 5(d)** shows the pattern obtained from the initial distribution provided in **Figure 5(a)**. V-shaped bundles, except for those in the transformed area, seemed to maintain a delicate balance and its own combination among bundles. Therefore, the correlation between the patterns shown in **Figure 5(a)** and **Figure 5(d)** was 5.53×10^{-2}, which was little less than the one without transformation. We independently performed image analysis, performed numerical simulation of the RD system with anisotropic diffusion, and calculated the correlations for 20 samples with single-area transformations.
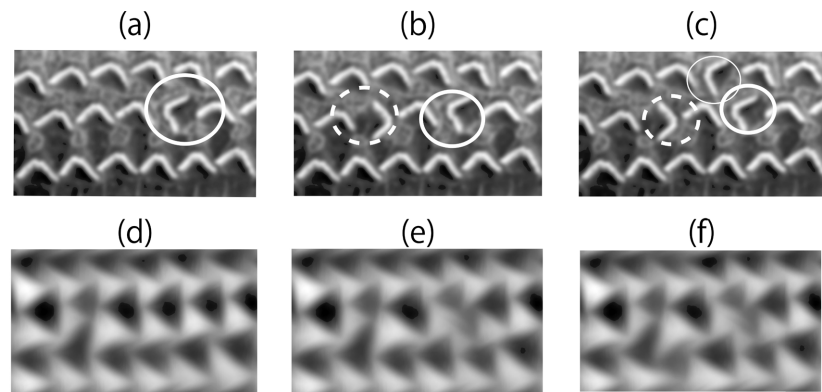
Figure 5. (a)-(c) Image analysis performed. (d)-(f) display the obtained patterns using the numerical simulation of Equations (5)-(7). Initial distributions are given by the distributions linearly transformed from −0.5 to 0.5 from the pixel data (a), (b), and (c), respectively.

Figure 5(b) and Figure 5(c) show examples of double- and triple-area transformations, respectively, in which the transformations performed are shown by white circles consisting of thick, thin, or dotted lines. Following the diagram shown in Figure 3, we obtained the RD patterns and the correlations. Figure 5(e) and Figure 5(f) show the patterns obtained from the initial distributions given in Figure 5(b) and Figure 5(c). Twenty samples were tested similar to those with double- or triple-area transformations.

Figure 6 shows the summary of the correlation changes in the number of transformation areas (single-area transformation: Ch1; double-area transformation: Ch2; and triple-area transformation: Ch3). The correlation score gradually decreased as the number of transformed areas increased. Significant differences in the number of deformation were observed.

3.3. Changes in Degree of Bending at the Apex of the V-Shaped Bundles

In this section, we examined the bending degree of deformation in which the V-shaped bundle pointed toward the portion observed in the part indicated by the brown arrow in Figure 4(b). The degree of the angled parts of the pointed part of the V-shaped bundle decreased as one pointed by "m1" to "m3" in Figure 4(b). Image analysis was performed to measure the quantitative differences during modified changes in the pointed parts of the V-shaped bundle. Figure 7 shows the summary of the transformation performed here. For example, in the control image (Figure 4(a)), the V-shaped bundle as indicated by "m1" in Figure 4(b) was embedded in the same area as the ones indicated by white circles in Figure 5. Then, numerical simulations were performed in the manner shown in Figure 3.

Table 2 shows the summary of the correlation I (Equation (8)). The degree and number of bending are gradually decreasing quantitatively using the correlation of Equation (8).
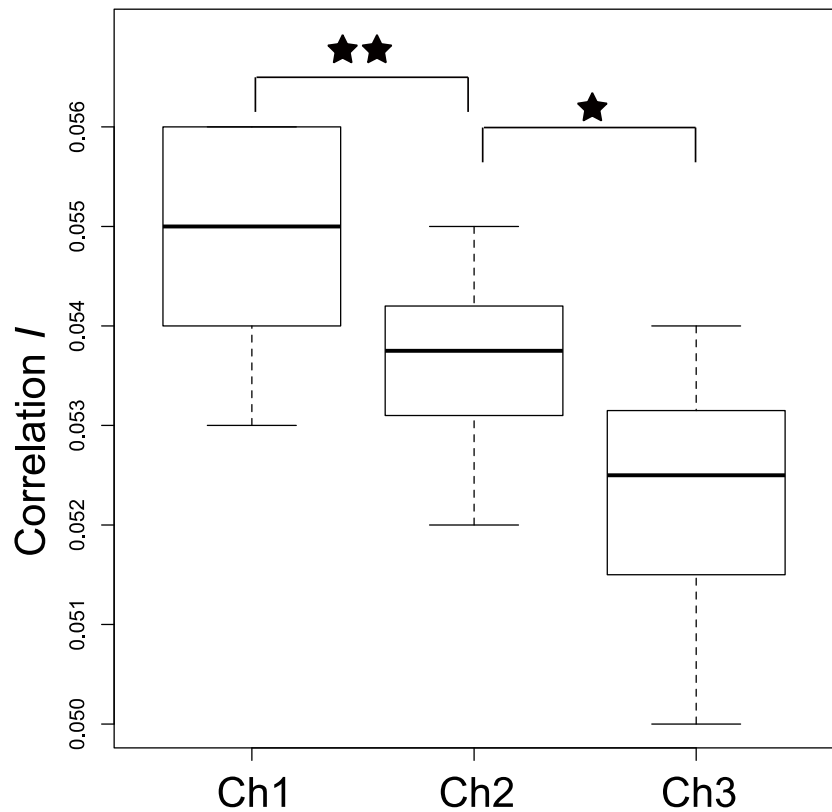
Figure 6. (a) Change in correlation I relative to the number of transformations. The number of stars indicates the statistical level of significance ($\bigstar$: $p < 0.05$, $\bigstar\bigstar$: $p < 0.01$). The Kruskal-Wallis test among Ch1, Ch2, and Ch3, $p = 1.72 \times 10^{-3}$. The Mann-Whitney U-test between Ch1 vs. Ch2, $p = 1.09 \times 10^{-3}$: Ch2 vs. Ch3, $p = 4.53 \times 10^{-2}$.
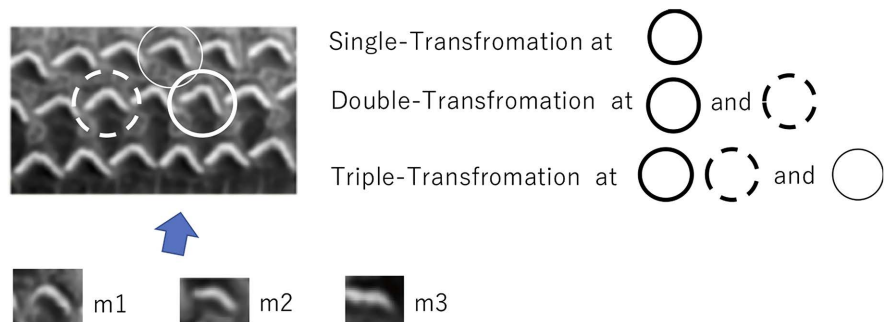

Figure 7. Transformations performed for gradual change of the degree of bending at the apex of the V-shaped bundles.

Table 2. The summary of the correlation I (Equation (8)) of transformed images explained in **Figure 7** and text.

	Single-area transformation	Double-area transformation	Triple-area transformation
m1	5.63×10^{-2}	5.58×10^{-2}	5.50×10^{-2}
m2	5.61×10^{-2}	5.52×10^{-2}	5.48×10^{-2}
m3	5.52×10^{-2}	5.44×10^{-2}	5.31×10^{-2}

4. Discussion

In this study, we developed a method for evaluating the V-shaped bundle patterns of outer cells using an RD system with anisotropic diffusion. Using the proposed RD model, quantitative differences were observed in the number of orientation changes of the V-shaped bundles and in the gradual change of degree at the apex of the V-shaped bundles.

The other advantage of this method was that the morphogenetic features were similar to biological pattern formation. The obtained triangular patterns adjusted the location to each other and arranged accordingly. That morphology is similar to the motility of outer hair cells and their electromotility [20] [21] [22].

Here, we comment on the change of correlation in Section 3.2. We also performed the image analysis of the images with more than four areas. As the number of transformation areas increased to more than four, correlation differences gradually decreased; however, no significant difference in the correlation I (Equation (8)) between triple- and quad-area transformations was detected. The increase in the number of transformations in images was not linearly reflected in the correlation I (Equation (8)); however, the pattern changes along with the surrounding bundles may change nonlinearly.

For effective orientation extraction of a given image, adjusting the parameters in the model is required to obtain patterns with a suitable frequency period of the given image. The parameters d_u and d_v are particularly useful for this purpose. A smaller d_v (larger d_u) implies a long period in which the RD system is generated. If the period of the numerically obtained pattern is different from the image to analyze, changing the parameters, especially d_u and d_v, is necessary. In this study, we set the parameters explained above, because the period of the pattern, which is equal to the number of V-shaped bundles in images, was fixed. Then, at each point, the orientation of the V-shaped bundles (**Figure 4(a)**) and triangle in the numerically obtained image (**Figure 4(f)**) are the same. As V-shaped bundles maintain a delicate balance and their own combination among bundles, the triangles exhibit balance and combination among the generated triangles.

Finally, the periodic patterns appearing in the biological and medical fields often included more localities than those appearing in physical or electric processes. Thus, the method proposed in this study can be useful for detecting periodicities in some localities. Therefore, the proposed method is expected to facilitate further analysis of periodic triangle patterns.

Acknowledgements

Conflicts of Interest

The authors declare no conflicts of interest regarding the publication of this paper.

References

[1] Turing, A.M. (1952) The Chemical Basis of Morphogenesis. *Philosophical Transactions of the Royal Society B*, **237**, 37-72. https://doi.org/10.1098/rstb.1952.0012

[2] Maini, P.K., Painter, K.J. and Chau, H.N.P. (1997) Spatial Pattern Formation in Chemical and Biological Systems. *Journal of the Chemical Society, Faraday Transactions*, **93**, 3601-3610. https://doi.org/10.1039/a702602a

[3] Murray, J.D. (1989) Mathematical Biology. Springer-Verlag, Berlin. https://doi.org/10.1007/978-3-662-08539-4

[4] DeKepper, P., Dulos, E., Boissonade, J., DeWit, A., Dewel, G. and Borckmans, P. (2000) Reaction-Diffusion Patterns in Confined Chemical Systems. *Journal of Statistical Physics*, **101**, 495-508. https://doi.org/10.1023/A:1026462105253

[5] Kondo, S. and Miura, T. (2010) Reaction-Diffusion Model as a Framework for Understanding Biological Pattern Formation. *Science*, **329**, 1616-1620. https://doi.org/10.1126/science.1179047

[6] Admatzky, A., Costello, B.D.K. and Asai, T. (2005) Reaction Diffusion Computers. Elsevier, Amsterdam.

[7] Ito, K., Aoki, T. and Higuchi, T. (2001) Digital Reaction-Diffusion System—A Foundation of Bio-Inspired Texture Image Processing. *IEICE Transactions on Fundamentals of Electronics*, **E84-A**, 1909-1918.

[8] Shoji, H. (2018) A Reaction-Diffusion Algorithm for Segmentation of Three-Dimensional Sinusoidal Networks in Rat Fed a High Fat and High Cholesterol Diet: New Insight and Evaluation. *Journal of Biosciences and Medicines*, **6**, 22-32. https://doi.org/10.4236/jbm.2018.610004

[9] Shoji, H., Yamada, K., Ueyama, D. and Ohta, T. (2007) Turing Patterns in Three Dimensions. *Physical Review E*, **75**, Article ID: 046212. https://doi.org/10.1103/PhysRevE.75.046212

[10] Abraham, L.K., Laura, L.T. (2019) Histology and Cell Biology: An Introduction to Pathology. 5th Edition, Elsevier Inc.

[11] Mescher, A.L. (2021) Junqueira's Basic Histology Text & Atlas. 16th Edition, McGraw Hill.

[12] Ciganovic, N., Wolde-Kidan, A. and Reichenbach, T. (2017) Hair Bundles of Cochlear Outer Hair Cells Are Shaped to Minimize Their Fluid-Dynamic Resistance. *Scientific Reports*, **7**, Article No. 3609. https://doi.org/10.1038/s41598-017-03773-y

[13] Hopkins, K. (2015) Deafness in Cochlear and Auditory Nerve Disorders. *Handbook of Clinical Neurology*, **129**, 479-494. https://doi.org/10.1016/B978-0-444-62630-1.00027-5

[14] Forge, A., Taylor, R.R., Dawson, S.J., Lovett, M. and Jagger, D.J. (2017) Disruption of *SorCS2* Reveals Differences in the Regulation of Stereociliary Bundle Formation between Hair Cell Types in the Inner Ear. *PLOS Genetics*, **13**, Article ID: e1006692. https://doi.org/10.1371/journal.pgen.1006692

[15] Gilels, F., Paquette, S.T., Beaulac, H.J., Bullen, A. and White, P.M. (2017) Severe Hearing Loss and Outer Hair Cell Death in Homozygous Foxo3 Knockout Mice after Moderate Noise Exposure. *Scientific Reports*, **7**, Article No. 1054. https://doi.org/10.1038/s41598-017-01142-3

[16] Fitzhugh, R. (1961) Impulses and Physiological States in Theoretical Models of Nerve Membrane. *Biophysical Journal*, **1**, 445-466. https://doi.org/10.1016/S0006-3495(61)86902-6

[17] Shoji, H., Iwasa, Y. and Kondo, S. (2003) Stripes, Spots, or Reversed Spots in Two-Dimensional Turing Systems. *Journal of Theoretical Biology*, **224**, 339-350. https://doi.org/10.1016/S0022-5193(03)00170-X

[18] Kobayashi, R. (1993) Modeling and Numerical Simulations of Dendritic Crystal Growth. *Physica D: Nonlinear Phenomena*, **63**, 410-423. https://doi.org/10.1016/0167-2789(93)90120-P

[19] Shoji, H., Iwasa, Y., Mochizuki, A. and Kondo, S. (2002) Directionality of Stripes Formed by Anisotropic Reaction-Diffusion Models. *Journal of Theoretical Biology*, **214**, 549-561. https://doi.org/10.1006/jtbi.2001.2480

[20] Brownell, W.E., Bader, C.R., Bertrand D. and de Ribaupierre. Y. (1985) Evoked Mechanical Responses of Isolated Cochlear Outer Hair Cells. *Science*, **227**, 194-196. https://doi.org/10.1126/science.3966153

[21] Kachar, B., Brownell, W.E., Altschuler, R. and Fex, J. (1986) Electrokinetic Shape Changes of Cochlear Outer Hair Cells. *Nature*, **322**, 365-368. https://doi.org/10.1038/322365a0

[22] Kalinec, F., Holley, M.C., Iwasa, K.H., Lim, D.J. and Kachar, B. (1992) A Membrane-Based Force Generation Mechanism in Auditory Sensory Cells. *Proceedings of the National Academy of Sciences of the United States of America*, **89**, 8671-8675. https://doi.org/10.1073/pnas.89.18.8671

[23] Siletti, K., Tarchini, B. and Hundspeth, A.J. (2017) Daple Coordinates Organ-Wide and Cell-Intrinsic Polarity to Pattern Inner-Ear Hair Bundles. *Proceedings of the National Academy of Sciences of the United States of America*, **114**, E11170-E11179. https://doi.org/10.1073/pnas.1716522115

[24] Ozono, Y., Tamura, A., Nakayama, S., Herawati, E., Hanada, Y., Ohata, K., Takagishi, M., Takahasi, M. Imai, T., Ohta, Y., Oshima, K., Sato, T., Inohara, H. and Tsukita, S. (2021) Daple Deficiency Causes Hearing Loss in Adult Mice by Inducing Defects in Cochlear Stereocilia and Apical Microtubules. *Scientific Reports*, **11**, Article No. 20224. https://doi.org/10.1038/s41598-021-96232-8